# Configurable Tendon Routing in a 3D-printed Soft Actuator for Improved Locomotion in a Multi-Legged Robot

Jose Barreiros[1], Kevin W. O'Brien[2], Samantha Hong[3], Michael F. Xiao[3], Ho-Jung Yang[3], and Robert F. Shepherd[2]

*Abstract*— **Soft robots struggle with terrestrial locomotion due to their inherent lack of rigidity, specifically along axes not in line with the direction of actuation (side loads). We present a method for improved stiffness in a 3D printed, tendon-driven soft actuator. We show, both mathematically and experimentally, that our method leads to improved stiffness to these side loads. Additionally, we demonstrate the use of complex tendon routing schemes to achieve various trajectories with a single actuator morphology. Finally, we demonstrate that these two tendon routing strategies lead to improved locomotion speed and gait efficiency in a 3-legged, 3D printed, soft robot.**

## I. INTRODUCTION

Soft actuators provide many potential benefits over their rigid counterparts including safer human interaction, behavioral diversity, and adaptability to unstructured environments [1, 2]. They have been used in a diverse range of applications including human performance augmentation, haptics, grasping, and locomotion [3, 4]. Due to their inherent compliance, these soft systems must exploit variable stiffness to achieve the benefits of low-modulus ($< 1$ GPa) materials while simultaneously having the ability to exert useful forces. There are many different actuation schemes common in the field of soft robotics which dynamically adjust an actuator's stiffness while causing motion and improving the ability to exert external forces (active stiffening). Some of the most common methods of active stiffening in soft systems are fluidic actuation [5–7], electroactive polymers [8, 9], shape memory materials [10, 11], and tendon-driven systems [12–16]. In this work, we focus on tendon-driven actuators due to the low size, weight, energy efficiency [17] and cost afforded by commodity geared dc motors [18].

Multiple methods of locomotion have been demonstrated in soft robots such as crawling, walking, jumping, vibration, wheel morphing, and tensegrity [2]. Even though some soft actuators are capable of exerting high forces [19, 20], they have not been used extensively for robotic walking due to their low stiffness in directions not directly opposing the actuator's motion. Soft materials inherently absorb and distribute forces which leads to difficulties in terrestrial locomotion due to the inability to transmit forces in a directed manner.

Additionally, there is evidence in nature that variable stiffness is needed to achieve terrestrial locomotion in soft-bodied biological systems. For example, spiders use hydraulics to change the stiffness of their leg joints to resist contraction and loads [21]. In caterpillars, cyclic changes in local stiffness along the body wall cause the undulatory behavior responsible for crawling and inching [22].

In this paper, we present a tendon-driven, soft actuator suitable for a walking robot. We use 3D printing of soft materials to create underactuated structures which are suitable for complex routings with multiple tendons. By using complex tendon routings, we exploit the multiplicity of degrees of freedom in our underactuated system to achieve varied limb trajectories from a single limb morphology driven by one motor. Additionally, we achieve increased resistance to axial loads by routing an array of tendons through parallel channels in the actuator. We first present the design and

*The first three authors contributed equally to this work.

**This work was supported by the Office of Naval Research under grant N00014-17-1-2837 and the Air Force Office of Scientific Research under grant FA9550-18-1-0243. Additionally, this work made use of the Cornell Center for Materials Research Shared Facilities, which are supported through the NSF MRSEC program (DMR-1719875)

***This paper has supplementary downloadable material available at http://ieeexplore.ieee.org, provided by the authors. This includes a multimedia AVI format movie clip, which show demonstrations of our device.

[1]Systems Science and Engineering, Cornell University, Ithaca, NY, USA jab879@cornell.edu

[2]Sibley School of Mechanical and Aerospace Engineering, Cornell University, Ithaca, NY, USA kwo6@cornell.edu, rfs247@cornell.edu

[3]Electrical and Computer Engineering, Cornell University, Ithaca, NY, USA sh974@cornell.edu, mfx2@cornell.edu, hy379@cornell.edu

manufacturing of the actuator. We then describe the achievable motions for different tendon routings and characterize the stiffness under axial load. We conclude with testing the capabilities of our actuator for terrestrial locomotion in a three legged-robot.

## II. Design and Manufacturing

Our 3D printed continuum actuator has a conical shape with five segments connected by a hollow cylinder (Fig. 1a). The actuator is designed to be driven by multiple tendons attached to a single motor. It also includes a stretchable optical waveguide [23] which (1) senses the degree of actuation and (2) serves as an antagonistic ligament which provides a return force during de-actuation.

Each of the five segments of the actuator contains two channels for stretchable optical waveguide placement and an array of channels along the outer radius to allow for routing multiple tendons in parallel and for complex routing schemes. We define complex tendon routing as a combination of straight and angled routing which, similar to longitudinal and oblique fibers in Cephalopod tentacles, allow for torsion and bending of the limb [24]. In this framework, a small change in the placement of elements (eg. tendon routing) leads to pre-programmed changes in the location of force application inside the body. These changes lead to a wider range of potential multiplane limb trajectories. Separately, parallel tendon routing provides improved actuator stiffness by increasing the moment arm of the tendon-generated torque resisting external axial loads.

In traditional rigid robots, proprioception is achieved at the individual joint level by using angular or linear position sensors (encoders, potentiometers, force gauges, etc). An underactuated soft-system, however, requires sensors that are capable of adapting to the conformation of the body. We chose to incorporate stretchable optical waveguides into our soft tentacle because of their high precision, repeatability, and linear response to elongation and bending [23].

We manufactured the actuators via Continuous Liquid Interface Production (CLIP), a type of commercial projection stereolithography (Fig. 1b). The actuators are printed from a low-modulus (~3 MPa) elastomeric polyurethane resin (EPU 40, Carbon Inc.). Each segment has a wall thickness of 1.5 mm and includes an internal lattice structure for support and increased compliance (Fig. 1c) (Video S1). After printing, a commercially available elastic urethane optical fiber [25] (Stretch Magic 1.5 mm, Pepperell Braiding Co.) is manually threaded through channels in the tentacle and bonded in place with EPU 40 resin. No cladding was used in the waveguide because the index of refraction of Stretch Magic (n ~1.52) is higher than that of air (n ~1).

Following thermal curing (8 hrs at 120° C), an infrared LED and phototransistor are friction fit into sockets within the actuator where they contact the ends of the optical waveguide (Fig. 1d). A brushed DC motor (298:1 Micro Metal Gearmotor HP 6V, Pololu Corporation) is attached to a spool (r = 2.5 mm) and enclosed in a rigid (~2 GPa) 3D printed box (Fig. 1e).

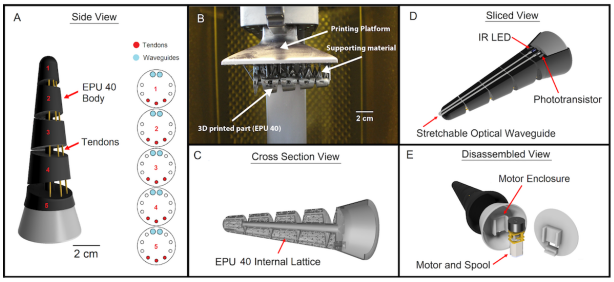


Fig. 1: (A) Schematic of the tendon-driven actuator including tendon and optical waveguide routing diagram. (B) The actuator on the printing platform with support material. (C) Cross-section view of the internal structure of the actuator. (D) View showing the internal stretchable optical waveguide for proprioception. (E) View showing the actuator with its internal motor and spool.

## III. Actuation

To characterize the performance of our actuator, we conducted three experiments. First, we tracked the trajectory of the actuator with different tendon routings. Second, we measured the stiffness of the actuator with axial loads along the circumference of the tip. Third, we measured the time-dependent response of the actuator, motor and its embedded sensor.

By routing tendons along different paths, our actuator achieves varying levels of bending and twisting (Fig. 2) (Video S2) which lead to complex motions across multiple planes. Fig. 3 shows the empirical data for the trajectory of four different tendon routing schemes, and additional trajectories

can be found in Appendix B. We captured videos of each trajectory from the front and the side of the actuator and tracked the position of the tip frame-by-frame using ImageJ.

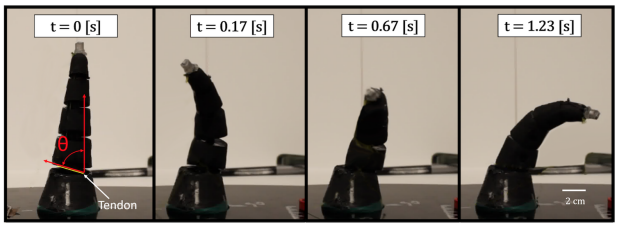


Fig. 2: A sequence of actuation showing bending and rotation of segments for complex routing.

The degree of rotation (twisting) of an actuator segment is directly related to the tendon routing angle, between the two consecutive segments. Additionally, the larger the routing angle, the higher the frictional force between the tendon and the routing channel. This friction leads to different trajectories for actuation and de-actuation in configurations with more drastic tendon routing angles, as can be seen in Fig. 3b,c,d.

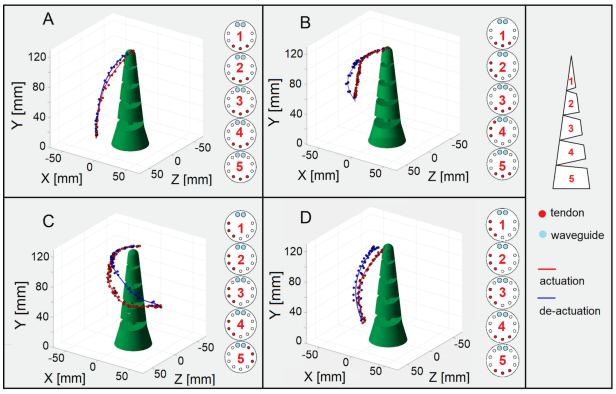


Fig. 3: Tentacle trajectories at different tendon routing schemes (A, B, C, D) showing actuation and de-actuation paths at the tip.

Our soft actuator dynamically increases its stiffness during actuation to transmit forces to the environment. During locomotion, it is important for the actuator to maintain sufficient resistance to side deflection such that actuation forces can be properly directed. When an external side load, $F$, is applied to our actuator (Fig. 4) a torque, $\tau_F$, is generated about the axis of rotation, $c$, between segments. This torque is balanced by the inherent elasticity of the elastomeric joint and waveguide, and the torque generated by the tendons. For a single tendon, this torque, $\tau_{TX1}$ is limited by the channel width, $w$. Alternatively, a system with three tendons can have an increased lever arm and therefore a higher balancing torque, $\tau_{TX3}$, to resist $\tau_F$. According to the proof below, based on a simplified model of a segment of the actuator, the balancing torque for a three-tendon system ($\tau_{TX3}$) will always be at least as high as that of a one-tendon system ($\tau_{TX1}$) under the condition at (10):

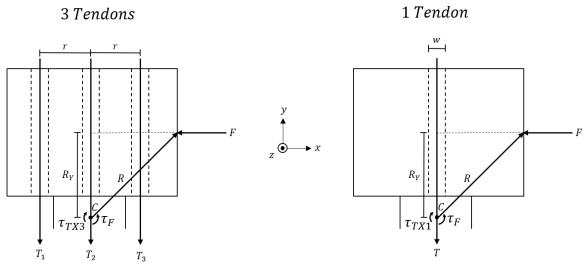


Fig. 4: Simplified model of a single actuator segment for stiffness analysis under a side load, $F$.

| **3 Tendon** | **1 Tendon** |
|---|---|
| (1) $\tau_F = F \cdot R_y$ | (3) $\tau_F = F \cdot R_y$ |
| (2) $\tau_{Tx_3} = (T_1 + T_3) \cdot r + T_2 \cdot \frac{w}{2}$ | (4) $\tau_{Tx_1} = T \cdot \frac{w}{2}$ |

(5) Assuming $\sum_{i=1}^{3} T_i = T$ ,

(6) $\tau_{Tx3} \iff \tau_{Tx1}$

(7) $T_1 \cdot r + T_x \frac{w}{2} + T_3 \cdot r \iff T_1 \frac{w}{2} + T_2 \frac{w}{2} + T_3 \frac{w}{2}$

(8) $(T_1 + T_3) \cdot r \iff (T_1 + T_3) \cdot \frac{w}{2}$

(9) $r \iff \frac{w}{2}$

(10) if $r > \frac{w}{2}$ $\therefore \tau_{Tx3} > \tau_{Tx1}$

This increase in stiffness to side loads, however, comes at the expense of reduced stiffness at angles normal to the direction of motion of the actuator (proof in Supplement A) as can be seen from the experimental data in Fig. 5 for an actuator with routing from Fig. 3d. This figure displays the difference in deflection between a single tendon and

three tendons routed in parallel in response to a load of ∼2.2 N at various angles, $\phi$, of force application. As expected, the data shows substantially less deflection to side loads (increased stiffness) with three tendons. The accompanying reduction in stiffness normal to the direction of motion can be seen in 5d (between 225 and 315 degrees) and 5e (between 180 and 315 degrees). This reduction in stiffness is less pronounced than the increase in stiffness to side loads. This is a welcome trade-off as the increased stiffness provided by multiple tendons is essential to terrestrial locomotion, as explored in Section IV.

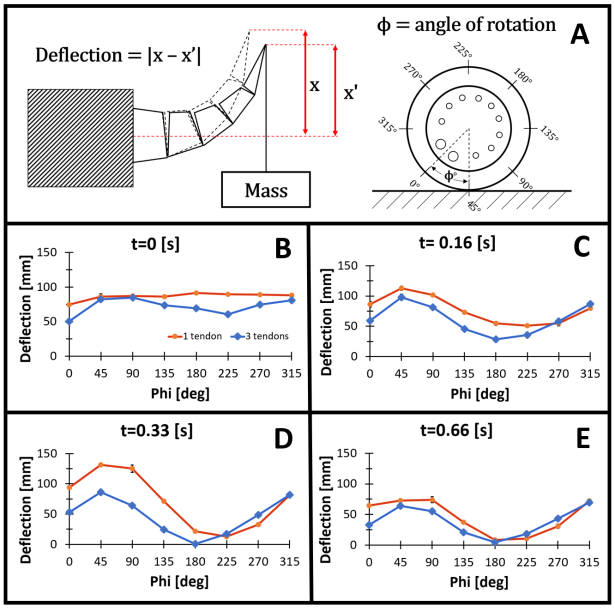


Fig. 5: (A) Schematic showing the experimental setup. (B, C, D, E) Deflection measurements of the tentacle tip at different base rotation angles, $\phi$, for 3-tendon routing and 1-tendon under a weight (220g) for increasing levels of actuation.

In Fig. 6, we show the time-dependent response of our tentacle (routing from Fig. 3d) including the tip position, waveguide reading, and motor current. Due to the viscoelastic nature of the polyurethane elastomers which comprise our actuator and embedded waveguide, they do not fully return to their original resting position within a reasonable time frame. To improve the repeatability of de-actuation, we added natural rubber strips (2.7 x 0.9 mm) parallel to the waveguide to increase return force and speed. The waveguide signal provides insight into the level of bending of the actuator which is used to determine the actuator's location in a gait cycle (discussed further in Section IV).

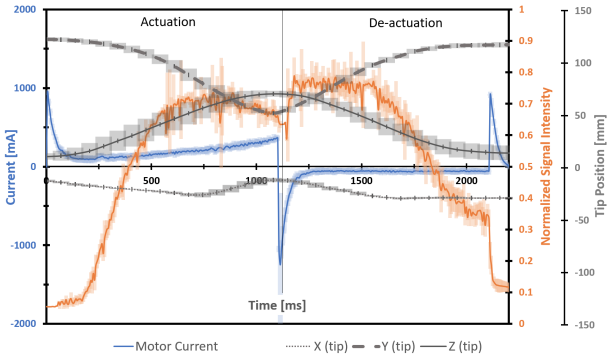


Fig. 6: Time response for a complete cycle of actuation showing X, Y, Z position at the tip of the actuator, waveguide signal, and motor current. The waveguide and rubber strip are antagonist components.

## IV. Implementation of the Soft Actuators in a Legged Robot

We incorporated three of our actuators into an untethered walking robot which consists of a soft body printed with EPU 40. The actuators are friction fit into the body and are equally spaced along its circumference (Fig. 7). The front actuator includes a silicone strip (Dragon Skin 10) at the tip to increase friction with the ground.

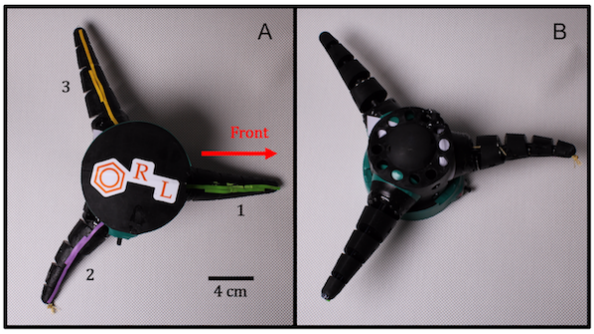


Fig. 7: (A) Top (B) Bottom of a 3-legged soft robot used for gait experiments.

The electronic system (Fig. 8) is based on a centralized architecture in which a microcontroller board (Teensy 3.2) interprets the signals from the phototransistor of each waveguide using a simple amplifier, as in [25], and controls the sequence of

actuation with a simple state machine. Fig. 9a, describes the state machine of a single leg of the robot. The sequence of actuation of the legs is controlled by the delay between the beginning of the cycle and the actuation of a leg, `delay_motor_n`, as shown in Fig 9b. The end of the actuation cycle (Motor moving clockwise "CC") of a leg is triggered at the event when the waveguide signal, `wguide_signal_n`, is greater than a given threshold, `wv_threshold_n`, that correlates with maximum actuation of the leg. To save the integrity of the system in the case the malfunction of the waveguide, the end of the actuation cycle is also triggered by a maximum actuation time, `CW_time`. The de-actuation of a leg (motor moving counter-clockwise "CCW") is limited to `CCW_time`, which is calculated online in every cycle and equals to the time that takes the leg to actuate to its full range (time passed from State 1 to State 2). All the electronics and battery are enclosed in a box at the top of the robot.

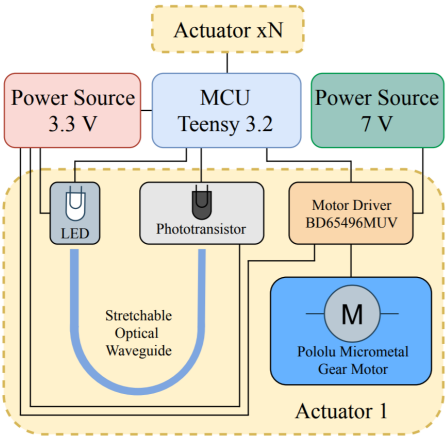


Fig. 8: System architecture for an N-legged robot.

We conducted a set of experiments with this robot to measure the effect of different tendon routing schemes on locomotion speed and gait efficiency. In this experiment, we set the robot on a rigid surface (tabletop) and measured the traveled distance, displacement, and speed with different tendon routings using ImageJ. For each tendon configuration, the robot used the same actuation sequence (Fig. 10) (Video S5) which was designed such that the robot would move in a straight path and relied on the waveguide signals to detect the end of each actuation cycle. This sequence was not optimized for our robot but, rather, was used as a baseline for comparison between different tendon routing configurations.

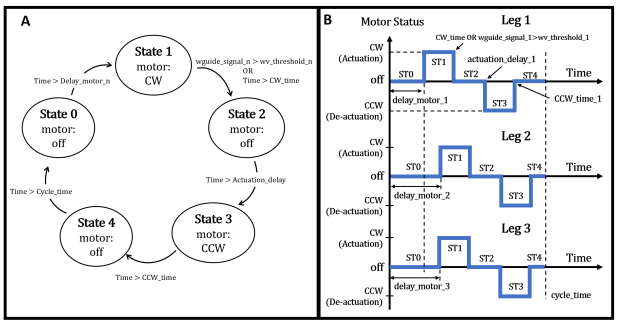


Fig. 9: (A) State Machine used to control a single leg. (B) Sequence of actuation of the legs used in the experiments.

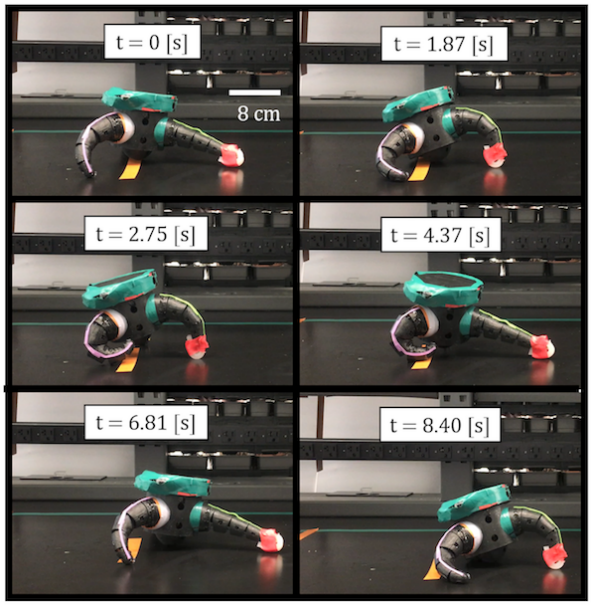


Fig. 10: Gait sequence of a 3 legged-robot on a rigid surface.

We used two metrics for our comparison (Table 1): speed, $s$, and efficiency ratio, $n$. The ratio, $n$, between the distance traveled, $d$, and the displacement of the robot, $r$, provide insight into the amount of energy wasted in locomotion which is not directed in a straight path. The velocity is defined as the displacement divided by time. From this data, we can see that the complex (curved) tendon routing provides an average increase of $s$ ~5.3 mm/s over the straight routing path and the increase from one to three tendons provides

an increase of $s$ ∼2.7 mm/s. Additionally, routing scheme D, which includes multiple tendons and complex routings, surpasses all other configurations we measured, in terms of both speed and efficiency ratio.

This increase in performance can be attributed to the increased stability from the additional stiffness provided by the multi-tendon actuators—the single-tendon configurations had difficulty maintaining balance during locomotion. Additionally, the configurations with complex routing outperformed straight routings largely due to (1) increased surface area contact with the ground at maximum actuation and (2) leg trajectories more aligned with the direction of motion of the robot.

TABLE I: Comparison of efficiency ratio and speed for gait at different schemes (4 trials each). Straight: routing from Fig. 3a. Curved: Leg 2 (routing from Fig. 3d) and Leg 3 (mirrored routing from Fig. 3d).

| Scheme | # of tendons | Leg 1 | Leg 2, 3 | Average Speed, $s$ (mm/s) | Efficiency ratio, $n$ |
|---|---|---|---|---|---|
| A | 1 | Straight | Straight | 2.17 ±2.77 | 0.24 ±0.05 |
| B | 1 | Straight | Curved | 8.15 ±1.38 | 0.12 ±0.05 |
| C | 3 | Straight | Straight | 5.55 ±1.03 | 0.12 ±0.07 |
| D | 3 | Straight | Curved | 10.17 ±1.79 | 0.33 ±0.03 |

## V. CONCLUSIONS

This paper has introduced a 3D printed tendon-driven soft actuator and a method of angled tendon routing for complex underactuated motion. We show that the multiplane motions achieved by this routing improve locomotion by combining bending and torsion. In addition, by utilizing a simple mathematical model and empirical evidence, we proved that multiple tendons routed in parallel result in increased stiffness to side loads, which when used in conjunction with complex tendon routings, further improves locomotion performance. Finally, we demonstrated that these tendon driven actuators are suitable for legged locomotion in a soft robot. The versatility of our 3D printed actuator allows for the possibility of multiple tendon routings which lead to a wide number of gait behaviors while keeping its morphology constant.

One limitation of the current embodiment of our actuator is that a single waveguide cannot fully interpret multiplane trajectories. For this reason, we will explore incorporating additional waveguides in future iterations. This increase in sensory feedback will create a multidimensional representation of the actuator conformation and will be used to generate adaptive gait algorithms. The use of additional waveguides will also serve to increase the return force and speed of the actuator—the return force and speed could further be increased by using silicone waveguides.

Additionally, in this study, we only explored the effect of two tendon routing schemes on locomotion. Further experiments with more routing schemes would be required to determine an optimal configuration for this robot. Finally, abrasion and tearing are challenges limiting the fatigue life of tendon-driven soft robots. These issues can be solved by introducing tendon channels with higher ultimate stress characteristics or by using tendons with elastic moduli closer to that of the robot's body.

## VI. APPENDIX

### A. Proof of Reduced Torque Normal to Direction of Motion

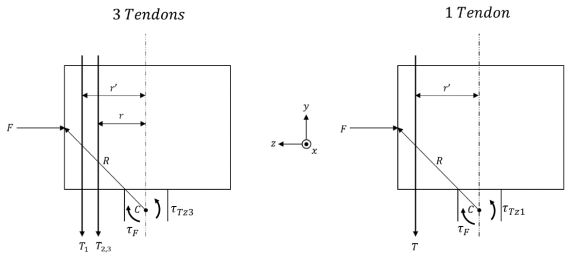


**3 Tendon** **1 Tendon**

(1) $\tau_F = F \cdot R_y$ (3) $\tau_F = F \cdot R_y$

(2) $\tau_{Fz_3} = (T_1 + T_3)r + T_2 \cdot r'$ (4) $\tau_{Fz_1} = T \cdot r'$

(5) Assuming $\sum_{i=1}^{3} T_i = T$,

(6) $\tau_{Tz3} \iff \tau_{Tz1}$

(7) $T_1 r + T_2 r' + T_3 r \iff T_1 r' + T_2 r' + T_3 r'$

(8) $(T_1 + T_3) \cdot r \iff (T_1 + T_3) \cdot r'$

(9) $r \iff r'$

(10) if $r < r'$ $\therefore \tau_{Tz3} < \tau_{Tz1}$

*B. Tentacle trajectories for different tendon routing schemes*

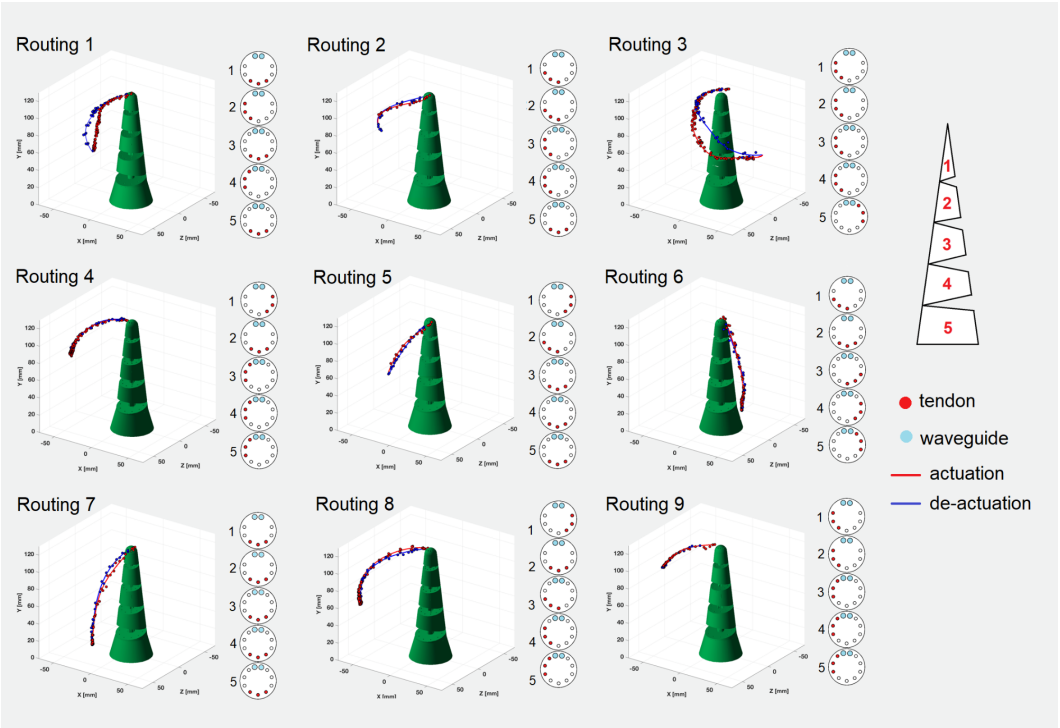


## References


[1] C. Laschi, B. Mazzolai, and M. Cianchetti, "Soft robotics: Technologies and systems pushing the boundaries of robot abilities," *Science Robotics*, vol. 1, p. eaah3690, 12 2016.

[2] M. Calisti, G. Picardi, and C. Laschi, "Fundamentals of soft robot locomotion," *Journal of The Royal Society Interface*, vol. 14, p. 20170101, 5 2017.

[3] P. Polygerinos, N. Correll, S. A. Morin, B. Mosadegh, C. D. Onal, K. Petersen, M. Cianchetti, M. T. Tolley, and R. F. Shepherd, "Soft Robotics: Review of Fluid-Driven Intrinsically Soft Devices; Manufacturing, Sensing, Control, and Applications in Human-Robot Interaction," 2017.

[4] C. Lee, M. Kim, Y. J. Kim, N. Hong, S. Ryu, H. J. Kim, and S. Kim, "Soft robot review," 2017.

[5] A. D. Marchese, R. K. Katzschmann, and D. Rus, "A Recipe for Soft Fluidic Elastomer Robots," *Soft Robotics*, 2015.

[6] T. J. Wallin, J. Pikul, and R. F. Shepherd, "3D printing of soft robotic systems," 2018.

[7] B. C. Mac Murray, X. An, S. S. Robinson, I. M. Van Meerbeek, K. W. O'Brien, H. Zhao, and R. F. Shepherd, "Poroelastic Foams for Simple Fabrication of Complex Soft Robots," *Advanced Materials*, 2015.

[8] E. Acome, S. K. Mitchell, T. G. Morrissey, M. B. Emmett, C. Benjamin, M. King, M. Radakovitz, and C. Keplinger, "Hydraulically amplified self-healing electrostatic actuators with muscle-like performance," *Science*, 2018.

[9] F. Carpi, D. De Rossi, R. Kornbluh, R. Pelrine, and P. Sommer-Larsen, *Dielectric Elastomers as Electromechanical Transducers*. 2008.

[10] M. Cianchetti, A. Licofonte, M. Follador, F. Rogai, and C. Laschi, "Bioinspired Soft Actuation System Using Shape Memory Alloys," *Actuators*, 2014.

[11] T. P. Chenal, J. C. Case, J. Paik, and R. K. Kramer, "Variable stiffness fabrics with embedded shape memory materials for wearable applications," in *IEEE International Conference on Intelligent Robots and Systems*, 2014.

[12] F. Maghooa, A. Stilli, Y. Noh, K. Althoefer, and H. A. Wurdemann, "Tendon and pressure actuation for a bio-inspired manipulator based on an antagonistic principle," in *Proceedings - IEEE International Conference on Robotics and Automation*, 2015.

[13] J. Reinecke, M. Chalon, W. Friedl, and M. Grebenstein, "Guiding effects and friction modeling for tendon driven systems," in *Proceedings - IEEE International Conference on Robotics and Automation*, 2014.

[14] F. Renda, M. Cianchetti, M. Giorelli, A. Arienti, and C. Laschi, "A 3D steady-state model of a tendon-driven continuum soft manipulator inspired by the octopus arm," *Bioinspiration and Biomimetics*, 2012.

[15] K. W. O'Brien, P. A. Xu, D. J. Levine, C. A. Aubin, H.-J. Yang, M. F. Xiao, L. W. Wiesner, and R. F. Shepherd, "Elastomeric passive transmission for autonomous force-velocity adaptation applied to 3D-printed prosthetics," *Science Robotics*, vol. 3, no. 23, 2018.

[16] V. Vikas, E. Cohen, R. Grassi, C. Sozer, and B. Trimmer, "Design and Locomotion Control of a Soft Robot Using Friction Manipulation and Motor–Tendon Actuation," *IEEE Transactions on Robotics*, vol. 32, pp. 949–959, 8 2016.

[17] J. L. Pons, E. Rocon, R. Ceres, D. Reynaerts, B. Saro, S. Levin, and W. Van Moorleghem, "The MANUS-HAND * Dextrous Robotics Upper Limb Prosthesis: Mechanical and Manipulation Aspects," tech. rep., 2004.

[18] T. Umedachi, V. Vikas, and B. A. Trimmer, "Softworms : the design and control of non-pneumatic, 3D-printed, deformable robots," *Bioinspiration & Biomimetics*, vol. 11, p. 025001, 3 2016.

[19] K. W. O'Brien, P. A. Xu, D. J. Levine, C. A. Aubin, H.-J. Yang, M. F. Xiao, L. W. Wiesner, and R. F. Shepherd,

"Elastomeric passive transmission for autonomous force-velocity adaptation applied to 3D-printed prosthetics," *Science Robotics*, vol. 3, 10 2018.

[20] B. Mosadegh, P. Polygerinos, C. Keplinger, S. Wennstedt, R. F. Shepherd, U. Gupta, J. Shim, K. Bertoldi, C. J. Walsh, and G. M. Whitesides, "Pneumatic networks for soft robotics that actuate rapidly," *Advanced Functional Materials*, 2014.

[21] D. a. Parry and R. H. J. Brown, "The Hydraulic Mechanism of the Spider Leg," *J. Exp. Biol.*, 1959.

[22] L. I. Van Griethuijsen and B. A. Trimmer, "Locomotion in caterpillars," *Biol. Rev*, vol. 89, pp. 656–670, 2014.

[23] H. Zhao, K. O'Brien, S. Li, and R. F. Shepherd, "Optoelectronically innervated soft prosthetic hand via stretchable optical waveguides," *Science Robotics*, vol. 1, p. eaai7529, 12 2016.

[24] W. M. Kier, "The Musculature of Coleoid Cephalopod Arms and Tentacles," *Frontiers in Cell and Developmental Biology*, 2016.

[25] C. K. Harnett, H. Zhao, and R. F. Shepherd, "Stretchable Optical Fibers: Threads for Strain-Sensitive Textiles," *Advanced Materials Technologies*, vol. 2, p. 1700087, 9 2017.